Wang, H. et al. (2013). Synthesis of carbon-supported PdSn-SnO_2 nanoparticles with different degrees of interfacial contact and enhanced catalytic activities for formic acid oxidation. Physical Chemistry Chemical Physics, 15: 13999
http://dx.doi.org/10.1039/c3cp52101j

Synthesis of carbon-supported PdSn–SnO_2 nanoparticles with different degrees of interfacial contact and enhanced catalytic activities for formic acid oxidation

Hui Wang, Ziyue Liu, Yanjiao Ma, Key Julian, Shan Ji, Vladimir Linkov and Rongfang Wang

Abstract

The conjunction of the PdSn alloy and SnO_2 is of interest for improving catalytic activity in formic acid oxidation (FAO). Here, we report the synthesis of PdSn–SnO_2 nanoparticles and a study of their catalytic FAO activity. Different degrees of interfacial contact between SnO_2 and PdSn were obtained using two different stabilizers (sodium citrate and EDTA) during the reduction process in catalyst preparation. Compared to the PdSn alloy, PdSn–SnO_2 supported on carbon black showed enhanced FAO catalytic activity due to the presence of SnO_2 species. It was also found that interfacial contact between the PdSn alloy and the SnO_2 phase has an impact on the activity towards CO oxidation and FAO.

1. Introduction

It is well established that Pd metal catalysts, being much less prone to CO poisoning and related deactivation, perform better than Pt catalysts in formic acid oxidation (FAO).[1–3] Combining Pd with a second noble metal component (such as Au,[4] Pt[5] and Ru,[6] *etc.*) is an effective way to enhance FAO activity, but the cost of such noble metal combinations still remains high. Consequently, Pd alloying with far cheaper non-noble metals (such as Fe,[7] Co,[8] Ni,[9–11] Cu,[12,13] and Sn[14–16]) has generated obvious interest, with steady improvements in catalytic activity and tolerance to CO poisoning being made through ongoing research.

Yet another promising route to enhance Pd catalyst activity is through the addition of transition metal oxides either as a component of the catalyst or as a support.[17–19] For example, both the catalytic FAO activity and CO tolerance of Pd/C catalysts have been enhanced through addition of MoO_x, which is attributed to the hydrogen spillover effect on MoO_x.[20,21] Similarly, SnO_2 as a support for the Pd catalyst has shown improved activity,[22] as has SnO_2 dispersed in polyindole which has reportedly good CO tolerance during FAO and follows a direct pathway to convert it into CO_2.[23]

In addition, other composite structures, where the alloy and metal oxide are in close proximity, such as the composite of RuO ·xH O with the PtRu alloy, have been reported to improve methanol oxidation activity in direct methanol fuel cells. Huang *et al.* reported enhanced PtRu/C catalyst activity by oxidation treatments resulting in the formation of intimate contact between RuO_2 crystalline phases and the PtRu alloy,[24,25] a phenomenon that has also been demonstrated elsewhere.[26] To further understand the relationship between the RuO_x and catalytic activity, Shyam *et al.* investigated the effect of RuO_x island size on the activity of the PtRu/C catalyst, and found that larger Ru islands were less susceptible to dissolution, induced a larger ligand effect, and were ultimately much more stable.[27] Given these observations, the effect of other metal oxides in such roles begs the need for similar thorough investigation.

In the present study, the effect of SnO_2 on PdSn activity in FAO was investigated. PdSn–SnO_2 and PdSn–SnO_2-island nano- particles supported on carbon were prepared by polyhydric alcohol reduction with different stabilizers. We report for the first time preparation of a hetero-structure, SnO_2 island, in intimate contact with PdSn nanoparticles, using a one-pot method. It was found that the degree of interfacial contact between PdSn and SnO_2 influences FOA catalytic performance, and that SnO_2 islands have a strong enhancing effect on catalyst activity.

2. Experimental procedures

2.1. Catalyst preparation

To prepare PdSn–SnO_2 supported on carbon (PdSn–SnO_2/C), 15.6 mg of $PdCl_2$ and 46.2 mg of $SnCl_4{\cdot}5H_2O$ were dissolved in 30 mL of EG in a 100 mL flask, followed by the addition of 288.2 mg of sodium citrate (stabilizer) with stirring for 0.5 h. Then, 100 mg of pretreated carbon black (Vulcan XC-72R) was added with pH adjusted to 10 by the drop-wise addition of a 5 wt% KOH– EG solution with vigorous stirring. The mixture was maintained at 160 1C for 8 h and the product collected by filtration, then washed four times with deionized water and finally dried in air at 60 1C for 5 h. To prepare PdSn–SnO_2-islands supported on carbon (PdSn–SnO_2-island/C), the above procedure and materials were used but with replacement of sodium citrate by 401.8 mg of ethylene diamine tetra-acetic acid (EDTA).

For a comparison, PdSn supported on carbon (PdSn/C), Pd/C and SnO_2/C catalysts were also prepared. PdSn/C was prepared as follows: palladium chloride ($PdCl_2$) (19.7 mg) was dissolved in a small amount of concentrated HCl to form H_2PdCl_4 aqueous solution, then stannic chloride pentahydrate ($SnCl_4{\cdot}\ 5H_2O$) (38.9 mg) dissolved in 30 mL ethylene glycol (EG) was added and stirred for 0.5 h. Pretreated carbon black Vulcan XC-72R (100 mg) was added to the mixture under stirring conditions and adjusted to pH E 9 by the drop-wise addition of a 5 wt% KOH–EG solution with vigorous stirring. The mixture was then maintained at 160 1C for 8 h, and the powder collected by filtration, washed several times with deionised water and dried in air at 60 1C for 5 h. The procedure for preparing

Pd/C is the same as the method used in the previous work[28] and the preparation of SnO_2/C is the same as the procedure used by Wang *et al.*[29]

2.2. Characterization

Particle size and morphology of the catalysts were analyzed by transmission electron microscopy (TEM) using a JEM-2010 microscope. X-ray diffraction (XRD) patterns of the catalysts were characterized on a Shimadzu XD-3A (Japan) goniometer, using Cu Ka radiation operated at 40 kV and 35 mA at room temperature. X-ray photoelectron spectroscopy (XPS) was carried out on a PHI-5702 multifunctional X-ray photoelectron spectrometer (American). The average chemical compositions of the catalysts were determined using an IRIS advantage inductively coupled plasma atomic emission spectroscopy (ICP-AES) system (Thermo, America).

Electrochemical tests were carried out on a CHI650D electro- chemical workstation. A conventional three-electrode cell was used, comprising a Ag/AgCl (3 mol L^{-1} KCl) reference electrode, a platinum wire counter electrode, and a modified glass carbon working electrode (5 mm in diameter). Before each measure- ment, the solution was saturated with N_2 gas. The catalyst ink was produced by mixing 5 mg of the catalyst ultrasonically in 1 mL Nafion–ethanol (0.25% Nafion). Catalyst layer preparations on the glassy carbon working electrode were made using 8 mL suspensions that were then dried in air. All measurements were made at ambient temperature.

3. Results and discussion

The XRD pattern of the PdSn–SnO_2/C catalyst prepared using sodium citrate as the stabilizer is shown in Fig. 1a. The diffraction peak at *ca.* 251 is associated with the (0 0 2) reflection of the hexagonal structure of Vulcan XC-72 carbon. The typical character of a crystalline Pd face-centered cubic (fcc) phase is confirmation of the (1 1 1), (2 0 0), (2 2 0), and (3 1 1) reflections at about 401, 471, 681 and 821, respectively.[30] The peaks located at 26.61 and 33.91 tetragonal SnO_2 phase, while the peak at 42.31 corresponds to the orthorhombic SnO_2 phase.[31,32] On the other hand, the (1 1 1) peak shifted to a slightly lower angle by E0.271, suggesting that Sn interacts with Pd resulting in Pd–Sn alloy formation.[33]

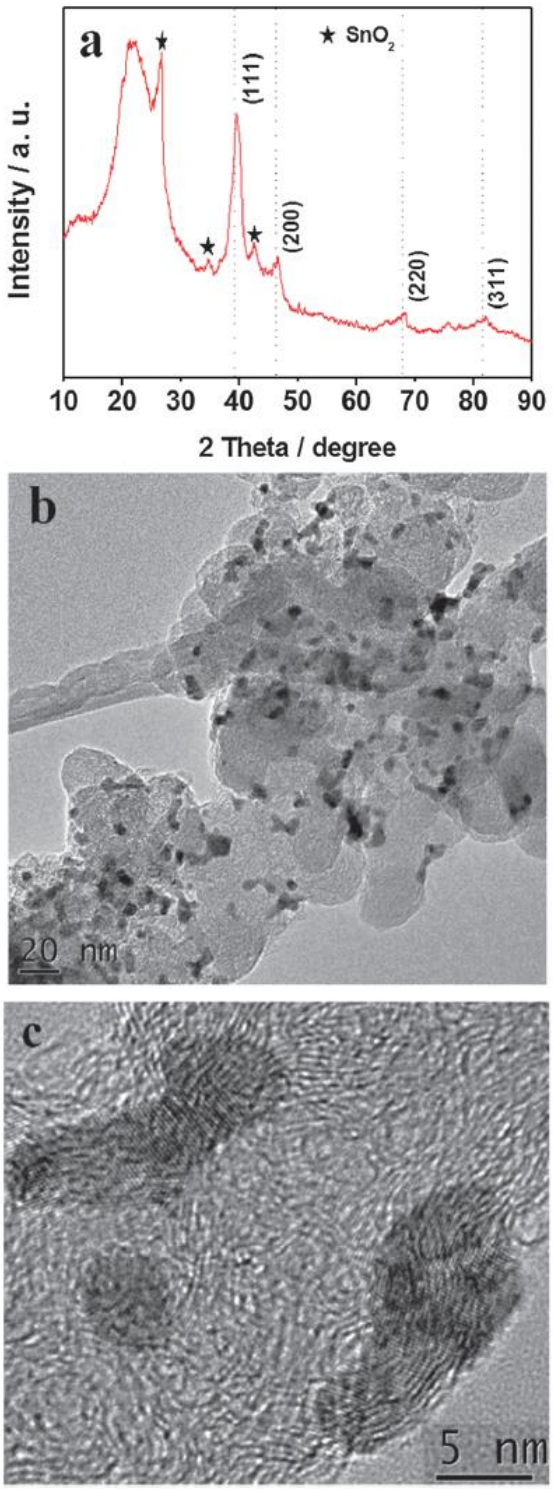

Fig. 1 (a) XRD pattern of the PdSn–SnO_2/C catalyst, the vertical dot lines represent the typical reflection of fcc Pd; (b) TEM and (c) HRTEM images of the PdSn–SnO_2/C catalyst.

The TEM image of PdSn–SnO_2/C (Fig. 1b) shows strip shaped catalyst nanoparticles homogeneously dispersed on the surface of carbon. The lengths of the strips range between 3 and 12 nm, with a width of ca. 3 nm. The fine structure of the strips was further characterized through high resolution transmission electron microscopy (HRTEM), as shown in Fig. 1c. We could not observe the grain boundaries in the strip. These results indicate that SnO_2 coexists with PdSn, which may be due to the crystal grains of SnO_2 being too small to be observed. From the above results, we can conclude that the composite structure of the PdSn–SnO_2/C catalyst with the strip morphology is formed and PdSn–SnO_2 is a PdSn alloy with phase-separated SnO_2. The interface between PdSn and SnO_2 is not observed. The composition of the catalyst was determined by ICP-AES analysis, with a metal loading of 19.7 wt% and a Pd : Sn atomic ratio of 1 : 1.47.

The XRD pattern of the PdSn–SnO_2-islands/C catalyst pre- pared using EDTA as the stabilizer is shown in Fig. 2a. The (0 0 2) reflection of carbon is observed at ca. 251 and the (1 1 1), (2 0 0), (2 2 0), and (3 1 1) reflections of fcc Pd at about 401, 471, 681 and 821, respectively. The weak reflections (marked with a black star) observed at 33.91 and 52.01 correspond to the (101) and (211) reflections of the tetragonal SnO_2 phase.[31,32] The peak located at 26.61, corresponding to the (1 1 0) reflection of the tetragonal SnO_2 phase, cannot be observed, perhaps because of the overlap with the (0 0 2) reflection of carbon. At the same time, a positive shift of ca. 0.201 for the (1 1 1) peak suggests the formation of the PdSn alloy.

The TEM image of the as-prepared PdSn–SnO_2-islands/C catalyst (see Fig. 2b) shows highly uniform dispersion of parti- cles with irregular sphere shaped morphology. However, we found that the very small particles connect with the edges of large particles (see particles illustrated with a red circle). The fine structure of the particles was further characterized using HRTEM, Fig. 2c and d. For observation, we choose two kinds of the particles, one lying between carbon particles (Fig. 2c), and the other located on the edge of carbon particles (see Fig. 2d). In Fig. 2c and d, the interfaces between PdSn and SnO_2 can be clearly seen, which indicates a hetero-structure, comprising SnO_2 islands in intimate contact with PdSn nanoparticles. It should be noted that the size of the SnO_2 islands is not uniform. Catalyst composition by ICP-AES analysis shows the metal load- ing to be 19.5 wt% with a Pd : Sn atomic ratio of 1 : 1.46.

The XRD pattern and TEM image of the prepared PdSn/C catalyst are shown in Fig. 3. The typical (1 1 1), (2 0 0), (2 2 0), and (3 1 1) reflections of fcc Pd can be seen in Fig. 3a, and the B0.251 positive shift confirms the formation of the PdSn alloy. Fig. 3b shows that the elliptical PdSn nanoparticles of 3–7 nm are uniformly dispersed on the surface of carbon black. The catalyst composition determined using ICP-AES analysis shows that the metal loading is 19.7 wt% with a Pd : Sn atomic ratio of 1 : 1.

XPS was employed to investigate the nature of surface species for the PdSn–SnO_2/C, PdSn–SnO_2-island/C and PdSn/C catalysts. The Pd 3d photoelectron core-level spectra of PdSn–SnO_2/C, PdSn–SnO_2-island/C and PdSn/C catalysts are shown in Fig. 4.

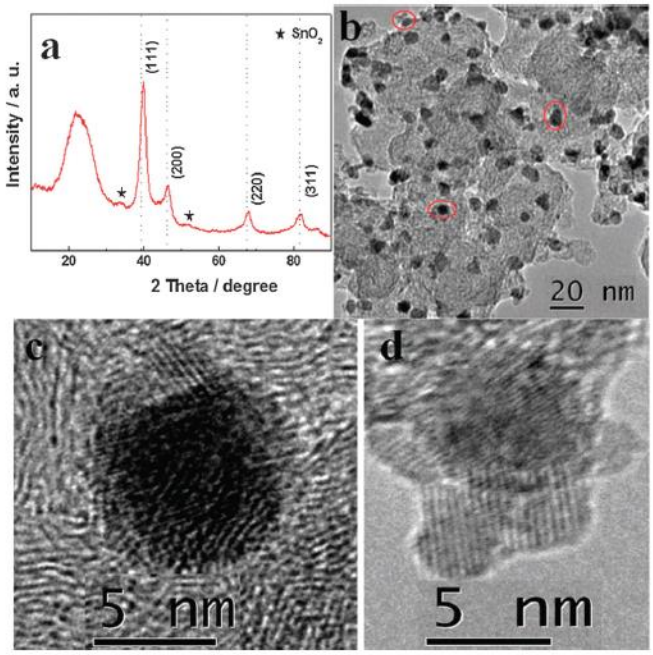

Fig. 2 (a) XRD pattern of the PdSn–SnO_2-islands/C catalyst, the vertical dot lines represent the typical reflection of fcc Pd; (b) TEM and (c and d) HRTEM images of the PdSn–SnO_2-islands/C catalyst.

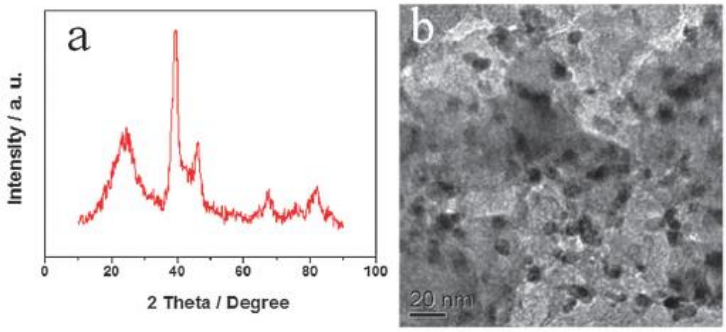

Fig. 3 (a) The XRD pattern and (b) TEM image of the PdSn/C catalyst.

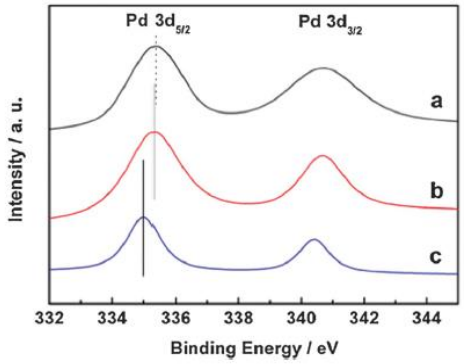

Fig. 4 XPS spectra for the Pd 3d core-level of the nanoparticles of the samples (a) PdSn–SnO_2-islands/C, (b) PdSn–SnO_2/C, and (c) PdSn/C. The maximum of the Pd $3d_{5/2}$ peak is used as the measure of the binding energy and is indicated by the vertical lines.

Table 1 Pd 3d and Sn $3d_{5/2}$ binding energy of the three catalysts

			Sn $3d_{5/2}$		
Catalyst	Pd $3d_{5/2}$/eV	Pd $3d_{3/2}$/eV	Sn(0)	Sn(II)	Sn(IV)
PdSn–SnO_2-islands/C	335.3	340.7	487.1	486.4	485.3
PdSn–SnO_2/C	335.2	340.4	487.2	486.2	485.3
PdSn/C	335.0	340.4	468.0	486.0	485.2
Pd[13]	335.1	—			

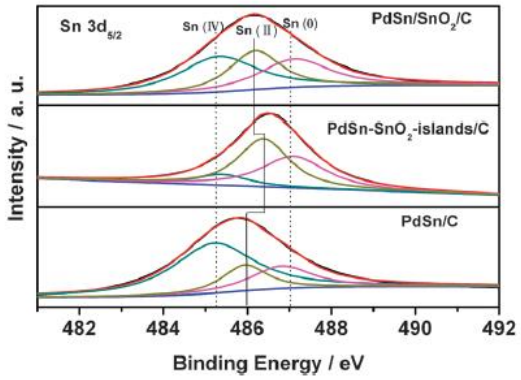

Fig. 5 Sn $3d_{5/2}$ core-level XPS spectra of PdSn–SnO_2/C, PdSn–SnO_2-islands/C and PdSn/C catalysts.

All of the spectra show two peaks corresponding to Pd $3d_{5/2}$ and Pd $3d_{3/2}$, which are characteristic peaks of Pd metal. The binding energies (BEs) of all peaks are listed in Table 1. Compared with the literature,[20–22] it is found that most of the Pd in the catalysts Fig. 5 Sn $3d_{5/2}$ core-level XPS spectra of PdSn–SnO_2/C, PdSn–SnO_2-islands/C and PdSn/C catalysts exists as metallic Pd and there is only a small amount of Pd oxide. The Pd metal is easily oxidized to form Pd oxide under ambient conditions.[20] Compared with the PdSn/C catalyst, positive shifts of BEs for PdSn–SnO_2/C and PdSn–SnO_2-islands/C catalysts are observed.

Based on the electronegativity series (Sn, 1.96; Pd, 2.20), the addition of Sn in the PdSn system means that charge transfer occurs from Sn to Pd, resulting in decrease in Pd BE, *i.e.* the negative shift of Pd 3d BE of PdSn. Moreover, the electronic effect of Sn increases with the increase of Sn content.[16] The Sn contents in PdSn–SnO_2/C and PdSn–SnO_2-islands/C catalysts are higher than that of the PdSn/C catalyst, but a positive shift of Pd 3d BE occurs. In the work of Feng *et al.*,[19] the interaction between Pd nanoparticles and the CeO_2 particles leads to the positive shift of the Pd 3d BEs. Similar results were also reported by other groups.[2,34,35] Here, it could be presumed that there is an interaction between the PdSn phase and the SnO_2 phase, *i.e.* the electronic structure of Pd is modified by both Sn species clearly shift to higher BE and follow in the order: Pd/C Pd/C o PdSn/C o PdSn–SnO_2/C o PdSn–SnO_2-islands/C. Changes in the Sn(II) 3d core-level BEs suggest that electronic modification of the Sn(II)O species by interactions with the PdSn substrate are dependent on the component.

The relative atomic percentages of different Sn species, determined from the related peak areas, are illustrated in Fig. 6. Due to the presence of the SnO_2 phase, the percentage of tin oxides in PdSn–SnO_2/C and PdSn–SnO_2-islands/C cata- lysts is much higher than that in the PdSn/C catalyst and the percentage of Sn(II) species for the PdSn–SnO_2-islands/C catalyst is obviously higher than the PdSn–SnO_2/C catalyst. Based on the results calculated from the atom superposition and electron delocalization molecular orbital theory, Anderson *et al.* proposed that the Sn(II)/Sn(IV) redox couple is the main factor for the generation of $(OH)_{ads}$, which can promote the oxidation of CO in the process of FAO.

Compared to PdSn/C, the offset of PdSn–SnO_2-islands/C is *ca.* 0.3 eV, which is larger than that of PdSn–SnO_2/C. The BE shifts depend on the extent of d-hybridization. d-Hybridization forms stronger bonds than the bonds between the metal atoms, which reduces the potential of the metal to form strong bonds with adsorbed reactants. In turn, this change of the adsorbing bond strength to a nanoparticle is a key factor for the reactivity.[36–38] Based on the above facts, the bonds with adsorbed reactants on PdSn–SnO_2-island nanoparticles would be weaker than PdSn–SnO_2 nanoparticles.

Sn $3d_{5/2}$ XPS spectra of the three catalysts are shown in Fig. 5. In order to better understand the contribution of different states of Sn atoms, XPS Sn $3d_{5/2}$ peaks were deconvoluted The peak fitting analysis of Sn $3d_{5/2}$ XPS data shows that there are three overlapped peaks; the one with the lowest BE corresponds to metallic Sn(0) ($3d_{5/2}$ = 485.3 ± 0.1 eV); the one with highest BE relates to fully oxidized Sn(IV) ($3d_{5/2}$ = 487.2 ± 0.1 eV) and the peak in between belongs to Sn(II) ($3d_{5/2}$ = 486.1 ± 0.5 eV).[39–41] The core-level BE difference of Sn(0), Sn(IV) and Sn(II) is consistent with values reported in the literature.[39–41] These results suggest the three Sn species existed on the surface for

all three catalysts. The existence of three Sn species was also reported under other experimental conditions.[40,42] As shown in Fig. 5, the Sn $3d_{5/2}$ peaks for Sn(II) species clearly shift to higher BE and follow in the order: Pd/C Pd/C o PdSn/C o PdSn–SnO_2/C o PdSn–SnO_2-islands/C. Changes in the Sn(II) 3d core-level BEs suggest that electronic modification of the Sn(II)O species by interactions with the PdSn substrate are dependent on the component.

The relative atomic percentages of different Sn species, determined from the related peak areas, are illustrated in Fig. 6. Due to the presence of the SnO_2 phase, the percentage of tin oxides in PdSn–SnO_2/C and PdSn–SnO_2-islands/C cata- lysts is much higher than that in the PdSn/C catalyst and the percentage of Sn(II) species for the PdSn–SnO_2-islands/C catalyst is obviously higher than the PdSn–SnO_2/C catalyst. Based on the results calculated from the atom superposition and electron delocalization molecular orbital theory, Anderson *et al.* proposed that the Sn(II)/Sn(IV) redox couple is the main factor for the generation of $(OH)_{ads}$, which can promote the oxidation of CO in the process of FAO.[43,44] Thus, it is expected that the different percentages of tin oxides lead to different activities for these three catalysts.

Fig. 7 shows the CO stripping voltammograms of the PdSn– SnO_2/C, PdSn–SnO_2-islands/C, PdSn/C, Pd/C and SnO_2/C cata- lysts, where CO was pre-adsorbed onto the different catalysts in a 0.5 mol L^{-1} H_2SO_4 solution for 5 min. It can be seen in Fig. 7 that adsorbed CO has been oxidized completely in the first scan, and no CO oxidation is monitored during the second scan for the PdSn–SnO_2/C, PdSn–SnO_2-islands/C, PdSn/C and Pd/C catalysts. SnO_2/C is not active for CO oxidation. The onset potentials of CO oxidation for the three catalysts follow in the order: PdSn–SnO_2-islands/C o PdSn–SnO_2/C o PdSn/C o Pd/C. The CO oxidation at the lower potential is mainly asso- ciated with the weakly adsorbed CO.[45] The result indicates that the existence of SnO_2 species can decrease the CO adsorption strength on PdSn particles. In addition, the peak potential of PdSn–SnO_2-islands/C has a more negative shift than that of PdSn–SnO_2/C, suggesting that PdSn–SnO_2-islands/C has better tolerance to CO than PdSn–SnO_2/C.

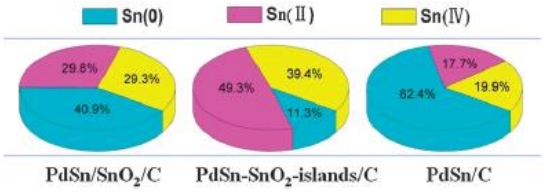

Fig. 6 Atomic ratio of Sn(0), Sn(II) and Sn(IV) species of the three catalysts.

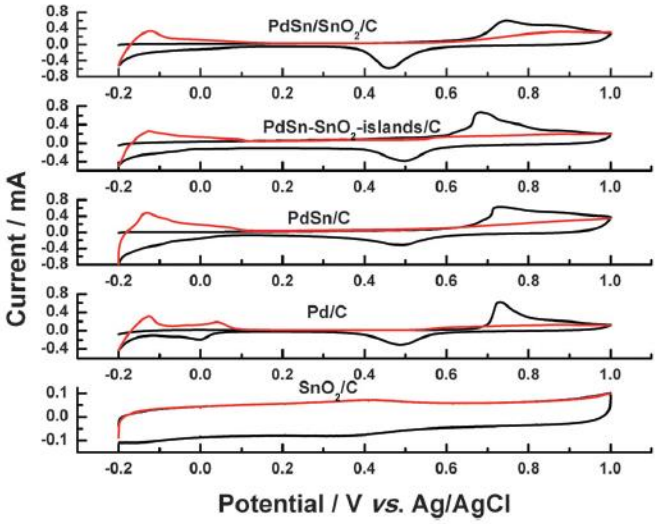

Fig. 7 The CO stripping voltammograms of the PdSn–SnO_2/C, PdSn–SnO_2-islands/C, PdSn/C, Pd/C and SnO_2/C catalysts in 0.5 mol L^{-1} H_2SO_4 solution at a scan rate of 50 mV s^{-1}.

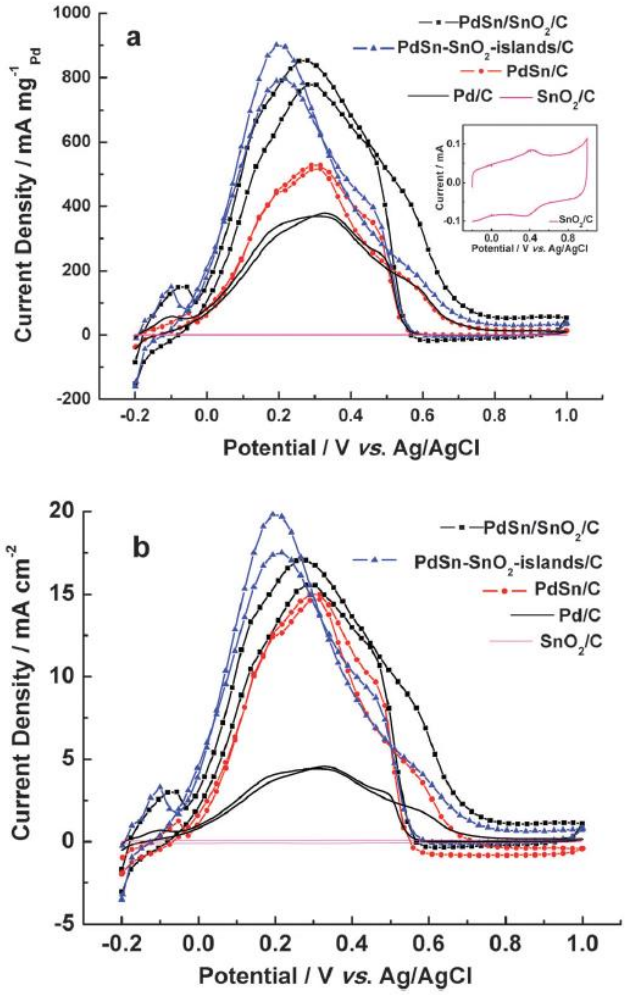

Fig. 8 Cyclic voltammograms of the PdSn–SnO_2/C, PdSn–SnO_2-islands/C, PdSn/C, Pd/C and SnO_2/C catalysts normalized to the Pd loading on the electrodes (a) and $ECSA_{CO}$ (b), in 0.5 mol L^{-1} HCOOH + 0.5 mol L^{-1} H_2SO_4 solution at a scan rate 50 mV s^{-1}.

Some reports have demonstrated that CO oxidation is improved by tin oxide *via* a bi-functional mechanism.[46,47] As discussed previously, the Sn(II)/Sn(IV) redox couple significantly affects the generation of OH_{ads}, resulting in enhanced activity of the catalysts.[43,44] The influence of Sn(II)/Sn(IV) on the catalytic activity and CO-tolerance were studied by Zhu's and White's groups.[39,48] Zhu *et al.* showed that ethanol electro-oxidation activity and CO tolerance can be obviously enhanced by increas- ing the Sn(II)/Sn(IV) ratio in the PtSn/C–Ni catalyst since the Sn(II)/ Sn(IV) redox couple accelerates the transfer rate of OH_{ads}.[48] White's group suggested that reduced Sn(II)O, rather than $Sn(IV)O_2$, is responsible for surface CO oxidation.[39] The Sn(II)/ Sn(IV) ratios obtained from Fig. 6 are *ca.* 1.0 for PdSn–SnO_2/C, *ca.* 1.3 for PdSn–SnO_2-islands/C and *ca.* 0.9 for PdSn/C, which result in the different CO-tolerance of these three catalysts.

The CO stripping curve was also used to evaluate the electrochemical surface area (ECSA).[49] The ECSA of each catalyst is listed in Table 2. The data indicate that the ECSA of PdSn–SnO_2-islands/C is close to that of PdSn–SnO_2/C, and their ECSAs are enhanced by a factor of *ca.* 1.5 and 1.9 compared with that of PdSn/C and Pd/C catalysts, respectively. Fig. 8 shows cyclic voltammograms (CVs) of 0.5 mol L^{-1} HCOOH in 0.5 mol L^{-1} H_2SO_4 ambient temperature. The CV of SnO_2/C is shown as an inset in Fig. 8a. It can be seen that SnO_2/C is not active for FAO, while two main peaks of the formic acid oxidation in both positive and negative scans with similar shapes were observed for all the other catalysts. In Fig. 8a and b, the peak potentials of PdSn–SnO_2/C, PdSn–SnO_2/C and PdSn/C are 0.18, 0.27, 0.30 and 0.31 V respectively, and the current density at 0.2 V (see Table 2) increases in the order: Pd/C o PdSn/C o PdSn– SnO_2/C o PdSn–SnO_2-islands/C. The high current density and low peak potential suggest that the existence of SnO_2 can enhance the catalytic activity of the PdSn alloy in FAO.[50]

Generally, the addition of SnO_2 to noble metals for use as electrocatalytic materials results in enhanced performance because SnO_2 may conveniently provide oxygen species to remove the CO-like species of oxidation residues, to free noble metal active sites.[51,52] This implies that the formation of the three-phase interface between SnO_2, H_2O and noble metal is key for enhanced FAO.[53] Kang *et al.* demonstrated that the contact between Au and FeO_x is the active region for CO oxidation, and that the activity is proportional to the amount of interfacial contact.[54] In the PdSn–SnO_2-islands/C catalyst, SnO_2 islands are in intimate contact with PdSn nanoparticles, which results in a high amount of the active sites and further leads to enhanced CO oxidation and FAO catalytic activity. However, it should be noted that SnO_2 islands in intimate contact with PdSn nanoparticles could also occupy some active sites on the PdSn surface, so the particle size of SnO islands should have an effect on the

catalytic activity. Therefore, according to the results of Kang *et al.*, further work is required to optimize the size of SnO_2 islands in the PdSn–SnO_2 system to maximize the catalytic activity in FAO.

Table 2 Electrochemical characterization of the three catalysts, the activities were obtained at 0.2 V

Catalyst	$ECSA_{CO}$ ($m^2\ g_{Pd}^{-1}$)	Mass activity ($mA\ mg_{Pd}^{-1}$)	Specific activity ($mA\ cm^{-2}$)
PdSn–SnO_2-islands/C	33.1	897.7	19.7
PdSn–SnO_2/C	35.2	777.6	15.6
PdSn/C	21.8	456.9	12.8
Pd/C	18.1	342.4	4.4

4. Conclusions

We have successfully prepared, *via* two different chemical reduction routes, PdSn–SnO_2/C nanoparticle catalysts with different degrees of interfacial contact. Using different stabilizers, the SnO_2 nanoparticles and hybrid PdSn–SnO_2 nanoparticles with different morphologies were obtained. PdSn–SnO_2/C catalysts were found to have substantially higher CO tolerance and catalytic activity for formic acid oxidation than PdSn alloy catalysts, mainly due to the presence of SnO_2. The different degrees of interfacial contact between PdSn and SnO_2 influenced the catalytic activity. These results may point to a new route for preparing novel hetero- structure electrocatalysts for fuel cells.

Acknowledgements

This work was financially supported by the NSFC (21163018) and NSFPSC (20110490847 and 2012T50554).

References

1. Y. Zhu, Z. Khan and R. I. Masel, *J. Power Sources*, 2005, 139, 15–20.

2. W.-L. Qu, Z.-B. Wang, Z.-Z. Jiang, D.-M. Gu and G.-P. Yin, *RSC Adv.*, 2012, 2, 344.
3. S. Ha, R. Larsen and R. I. Masel, *J. Power Sources*, 2005, 144, 28–34.
4. W. Zhou and J. Y. Lee, *Electrochem. Commun.*, 2007, 9, 1725–1729.
5. Y. Kang, L. Qi, M. Li, R. E. Diaz, D. Su, R. R. Adzic, E. Stach, J. Li and C. B. Murray, *ACS Nano*, 2012, 6, 2818–2825.
6. Z. L. Liu, X. H. Zhang and S. W. Tay, *J. Solid State Electro- chem.*, 2012, 16, 545–550.
7. J. Zhang, H. Yang, K. Yang, J. Fang, S. Zou, Z. Luo, H. Wang, I.-T. Bae and D. Y. Jung, *Adv. Funct. Mater.*, 2010, 20, 3727–3733.
8. M. Hakamada and M. Mabuchi, *Mater. Trans.*, 2009, 50, 431–435.
9. Y. Gao, G. Wang, B. Wu, C. Deng and Y. Gao, *J. Appl. Electrochem.*, 2011, 41, 1–6.
10. C. Du, M. Chen, W. Wang, G. Yin and P. Shi, *Electrochem. Commun.*, 2010, 12, 843–846.
11. C. Du, M. Chen, W. Wang and G. Yin, *ACS Appl. Mater. Interfaces*, 2010, 3, 105–109.
12. V. Mazumder, M. Chi, M. N. Mankin, Y. Liu, O. Metin, D. Sun, K. L. More and S. Sun, *Nano Lett.*, 2012, 12, 1102–1106.
13. C. Xu, Y. Liu, J. Wang, H. Geng and H. Qiu, *J. Power Sources*, 2012, 199, 124–131.
14. D. Tu, B. Wu, B. Wang, C. Deng and Y. Gao, *Appl. Catal., B*, 2011, 103, 163–168.
15. Z. Liu and X. Zhang, *Electrochem. Commun.*, 2009, 11, 1667–1670.
16. Z. Zhang, J. Ge, L. Ma, J. Liao, T. Lu and W. Xing, *Fuel Cells*, 2009, 9, 114–120.
17. W. Xu, Y. Gao, T. Lu, Y. Tang and B. Wu, *Catal. Lett.*, 2009, 130, 312–317.
18. L. P. R. Profeti, F. C. Simõ es, P. Olivi, K. B. Kokoh, C. Coutanceau, J. M. L´eger and C. Lamy, *J. Power Sources*, 2006, 158, 1195–1201.
19. L. Feng, J. Yang, Y. Hu, J. Zhu, C. Liu and W. Xing, *Int. J. Hydrogen Energy*, 2012, 37, 4812–4818.
20. R. Li, H. Hao, T. Huang and A. Yu, *Electrochim. Acta*, 2012, 76, 292–299.
21. L. Feng, Z. Cui, L. Yan, W. Xing and C. Liu, *Electrochim. Acta*, 2011, 56, 2051–2056.
22. H. Lu, Y. Fan, P. Huang and D. Xu, *J. Power Sources*, 2012, 215, 48–52.
23. A. Kumar, A. C. Pandey and R. Prakash, *Catal. Sci. Technol.*, 2012, 2, 2533–2538.
24. S. Huang, S. Chang, C. Lin, C. Chen and C. Yeh, *J. Phys. Chem. B*, 2006, 110, 23300–23305.
25. S. Huang, C. Chang, K. Wang and C. Yeh, *ChemPhysChem*, 2007, 8, 1774–1777.
26. Y.-C. Wei, C.-W. Liu, W.-J. Chang and K.-W. Wang, *J. Alloys Compd.*, 2011, 509, 535–541.
27. B. Shyam, T. M. Arruda, S. Mukejee and D. E. Ramaker, *J. Phys. Chem. C*, 2009, 113, 19713–19721.
28. K. Wang, H. Wang, R. Wang, J. Key, V. Linkov and S. Ji, *S. Afr. J. Chem.*, 2013, 66, 86–91.
29. W. Wang, Y. Li and H. Wang, *Micro Nano Lett.*, 2013, 8, 23–26.
30. J. C. Jia, R. F. Wang, H. Wang, S. Ji, J. Key, V. Linkov, K. Shi and Z. Q. Lei, *Catal. Commun.*, 2011, 16, 60–63.
31. Ü. Kersen and L. Holappa, *Anal. Chim. Acta*, 2006, 562, 110–114.
32. M.-R. Yang, S.-Y. Chu and R.-C. Chang, *Sens. Actuators, B*, 2007, 122, 269–273.
33. R. Awasthi and R. N. Singh, *Int. J. Hydrogen Energy*, 2012, 37, 2103–2110.
34. X. Zhao, J. Zhu, L. Liang, C. Liu, J. Liao and W. Xing, *J. Power Sources*, 2012, 210, 392–396.

35. M. Yin, Q. Li, J. O. Jensen, Y. Huang, L. N. Cleemann, N. J. Bjerrum and W. Xing, *J. Power Sources*, 2012, 219, 106–111.
36. X. Zhang, H. Wang, J. Key, V. Linkov, S. Ji, X. Wang, Z. Lei and R. Wang, *J. Electrochem. Soc.*, 2012, 159, B270–B276.
37. X. Mao, L. Yang, J. Yang, J. Key, S. Ji, H. Wang and R. Wang, *J. Electrochem. Soc.*, 2013, 160, H219–H223.
38. W. P. Zhou, A. Lewera, R. Larsen, R. I. Masel, P. S. Bagus and Wieckowski, *J. Phys. Chem. B*, 2006, 110, 13393–13398.
39. S. Axnanda, W. P. Zhou and M. G. White, *Phys. Chem. Chem. Phys.*, 2012, 14, 10207–10214.
40. W.-P. Zhou, S. Axnanda, M. G. White, R. R. Adzic and J. Hrbek, *J. Phys. Chem. C*, 2011, 115, 16467–16473.
41. L. Kover, Zs. Kovacs, R. Sanjines, G. Moretti, I. Cserny, G. Margaritondo, J. Palinkas and H. Adachi, *Surf. Interface Anal.*, 1995, 23, 461–466.
42. W. Du, K. E. Mackenzie, D. F. Milano, N. A. Deskins, D. Su and X. Teng, *ACS Catal.*, 2012, 2, 287–297.
43. A. B. Anderson, E. Grantscharova and P. Shiller, *J. Electrochem. Soc.*, 1995, 142, 1880–1884.
44. A. B. Anderson, S. Seong and E. Grantscharova, *J. Phys. Chem.*, 1996, 100, 17535–17538.
45. Y. Kim, H. J. Kim, Y. S. Kim, S. M. Choi, M. H. Seo and W. B. Kim, *J. Phys. Chem. C*, 2012, 116, 18093–18100.
46. M. Arenz, V. Stamenkovic, B. Blizanac, K. Mayrhofer, N. Markovic and P. Ross, *J. Catal.*, 2005, 232, 402–410.
47. Y. Ishikawa, M.-S. Liao and C. R. Cabera, *Surf. Sci.*, 2000, 463, 66–80.
48. M. Zhu, G. Sun, H. Li, L. Cao and Q. Xin, *Chin. J. Catal.*, 2008, 29, 765–770.
49. R. F. Wang, B. X. Wei, H. Wang, S. Ji, J. Key, X. T. Zhang and Z. Q. Lei, *Ionics*, 2011, 17, 595–601.
50. L. Feng, L. Yan, Z. Cui, C. Liu and W. Xing, *J. Power Sources*, 2011, 196, 2469–2474.
51. E. Antolini, F. Colmati and E. R. Gonzalez, *J. Power Sources*, 2009, 193, 555–561.
52. Z. Liu, D. Reed, G. Kwon, M. Shamsuzzoha and D. K. Nikles, *J. Phys. Chem. C*, 2007, 111, 14223–14229.
53. S. Chen, R. Si, E. Taylor, J. Janzen and J. Chen, *J. Phys. Chem. C*, 2012, 116, 12969–12976.
54. Y. Kang, X. Ye, J. Chen, L. Qi, R. E. Diaz, V. Doan-Nguye, G. Xing, C. R. Kagan, J. Li, R. J. Gorte, E. A. Stach and B. Murray, *J. Am. Chem. Soc.*, 2013, 135, 1499–1505.